Supporting Information

An ultra-broad-range pressure sensor based on gradient stiffness design

Fuhua Xue[1,§], Haowen Zheng[1,§], Qingyu Peng[1,3,*], Ying Hu[2,*], Xu Zhao[1], Liangliang Xu[1], Pengyang Li[1], Yue Zhu[1], Zonglin Liu[1] & Xiaodong He[1,3,*]

[1] National Key Laboratory of Science and Technology on Advanced Composites in Special Environments, Center for Composite Materials and Structures, Harbin Institute of Technology, Harbin 150080, P. R. China

[2] Institute of Industry & Equipment Technology, Hefei University of Technology, Hefei 230009, P. R. China

[3] Shenzhen STRONG Advanced Materials Research Institute Co., Ltd., Shenzhen 518000, P. R. China

* Corresponding authors. Email: pengqingyu@hit.edu.cn, huying@hfut.edu.cn, hexd@hit.edu.cn

[§]These authors contributed equally to this work.

Supplementary Figures

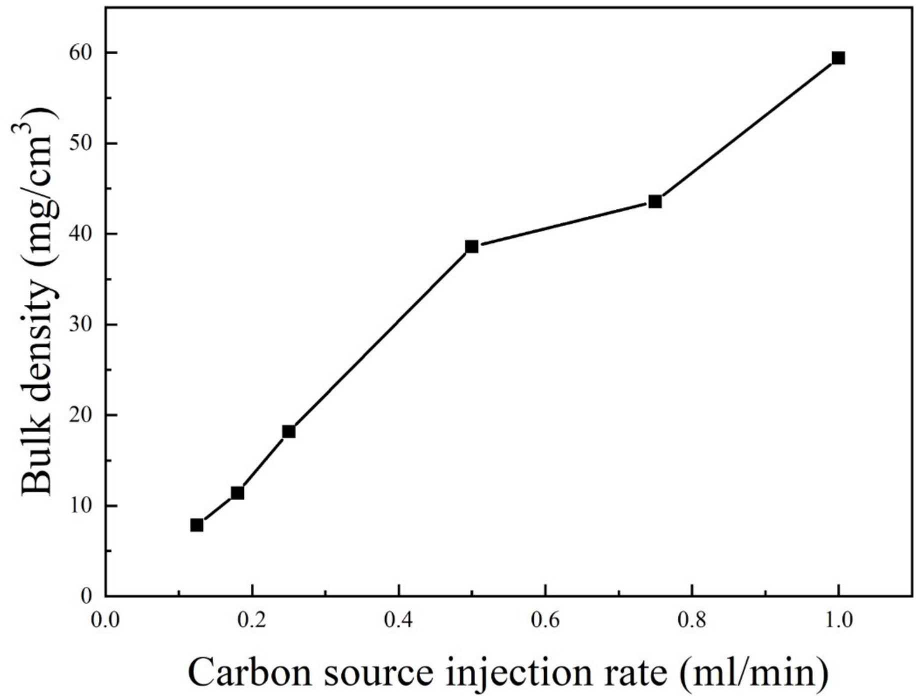

Figure S1. The bulk density of single-density carbon nanotube sponge increases with the increase of the carbon source solution injection rate.

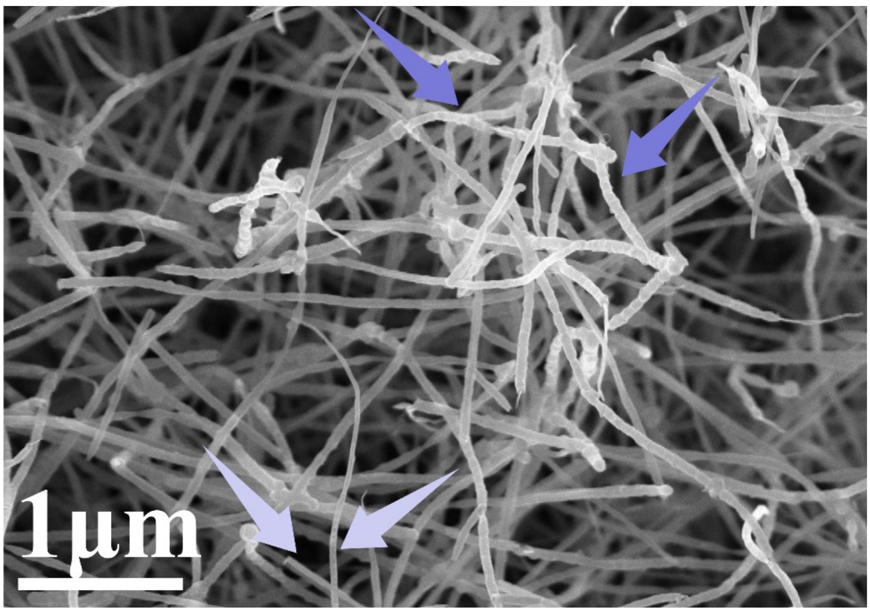

Figure S2. SEM image of the transition part between the high-density layer and the low-density layer

The light-colored arrows refer to the small-diameter CNTs with smooth surfaces, while the dark-colored arrows refer to the large-diameter CNTs with amorphous carbon attached to the surfaces.

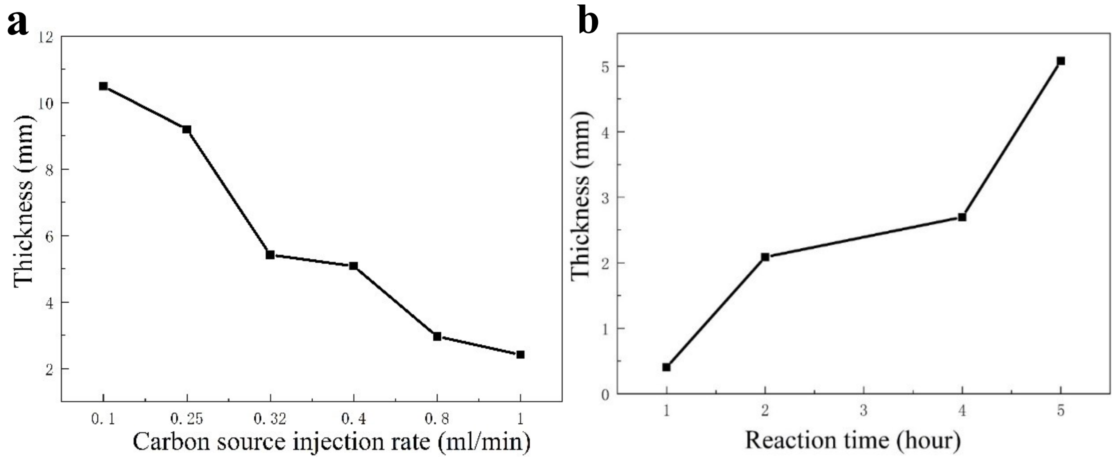

Figure S3. (a) The relationship between the thickness of the CNT sponge and the injection rate of the carbon source solution under the same reaction time of 5 hours. (b) The relationship between the thickness of the CNT sponge and the reaction time when the injection rate of the carbon source solution was fixed at 0.4ml/min.

We tested the relationship between the thickness of the CNT sponge and the injection rate of the carbon source solution under the same reaction time of 5 hours, as shown in the Figure S3(a). It can be found that the thickness of the resulting CNT sponge decreases as the injection rate of the carbon source solution increases. This is due to the increase in the number of CNTs tube walls, the number density of CNTs and the increase of amorphous carbon in the microscopic view. Afterward, we investigated the relationship between the thickness of the CNT sponge and the reaction time when the injection rate of the carbon source solution was fixed at 0.4ml/min. Because the thickness of the sponge cannot be observed in real time during the reaction process, we conducted four experiments which were reacted for 1h, 2h, 4h and 5h respectively. The relationship between the thickness of the CNT sponge and the reaction time is shown in the Figure S3(b). The thickness increases with the increase of the reaction time.

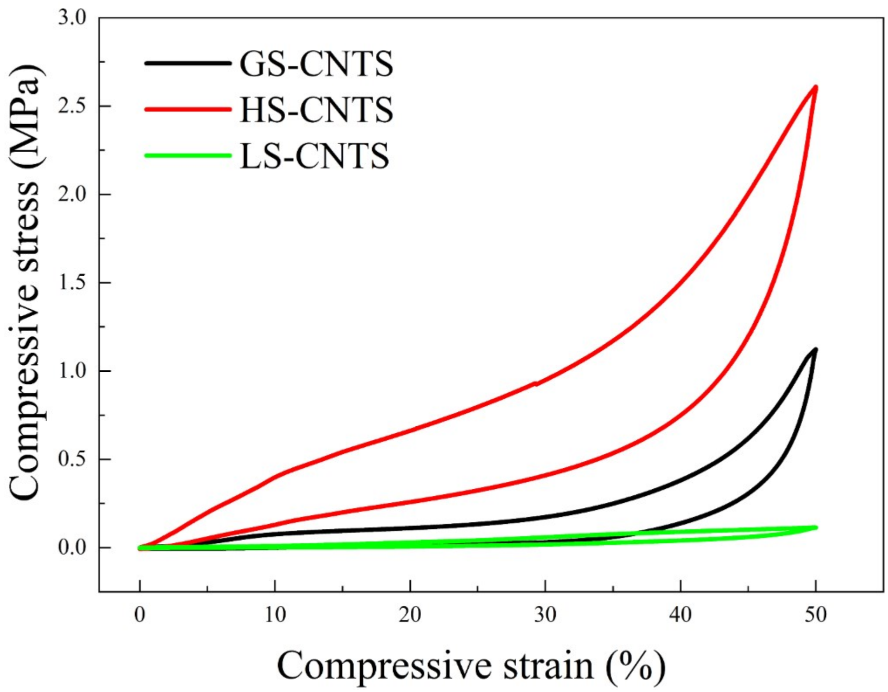

Figure S4. Compression stress-strain curves of the GS-CNTS, single HS-CNTS and single LS-CNTS.

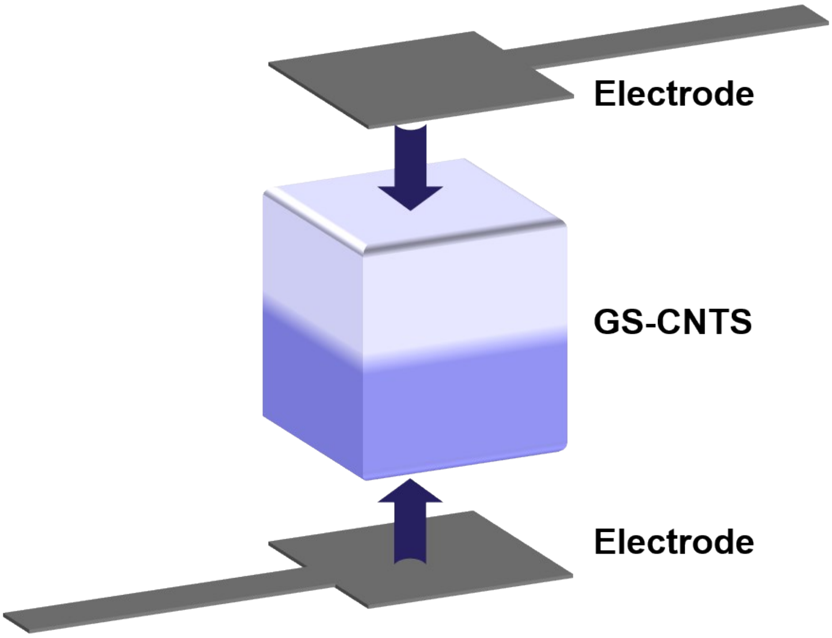

Figure S5. The schematic for the entire sensor structure including electrodes

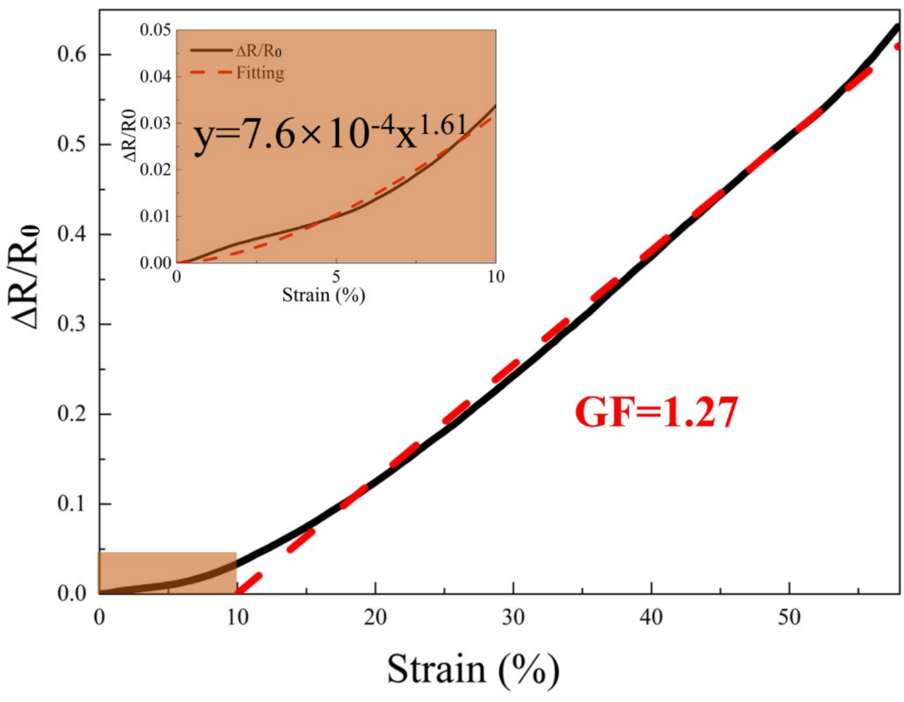

Figure S6. $\Delta R/R_0$ of the GS-CNTS as a function of compression strain.

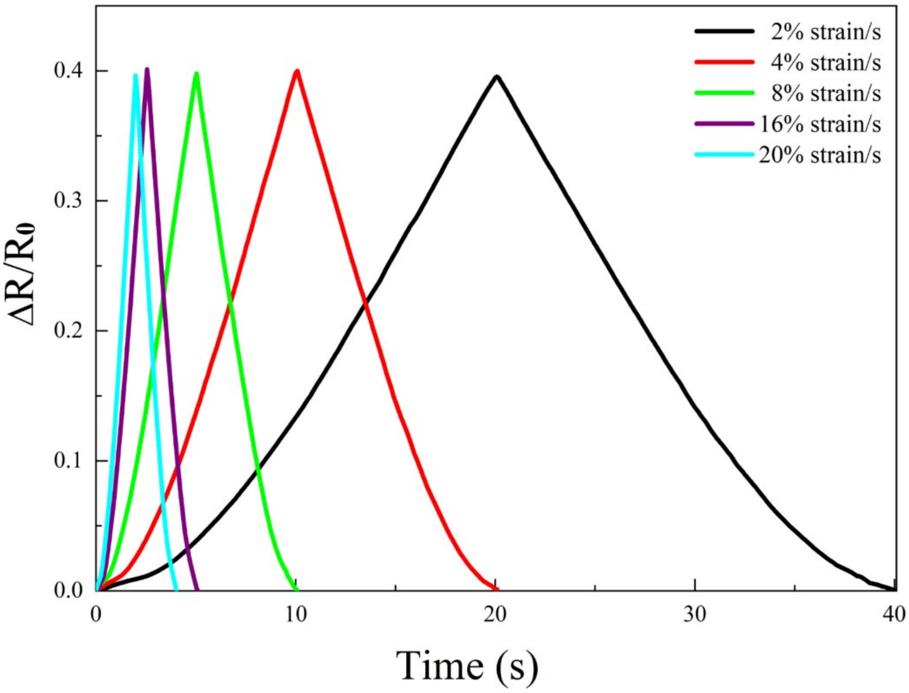

Figure S7. $\Delta R/R_0$-time curves of the GS-CNTS at various frequencies under a 40% strain.

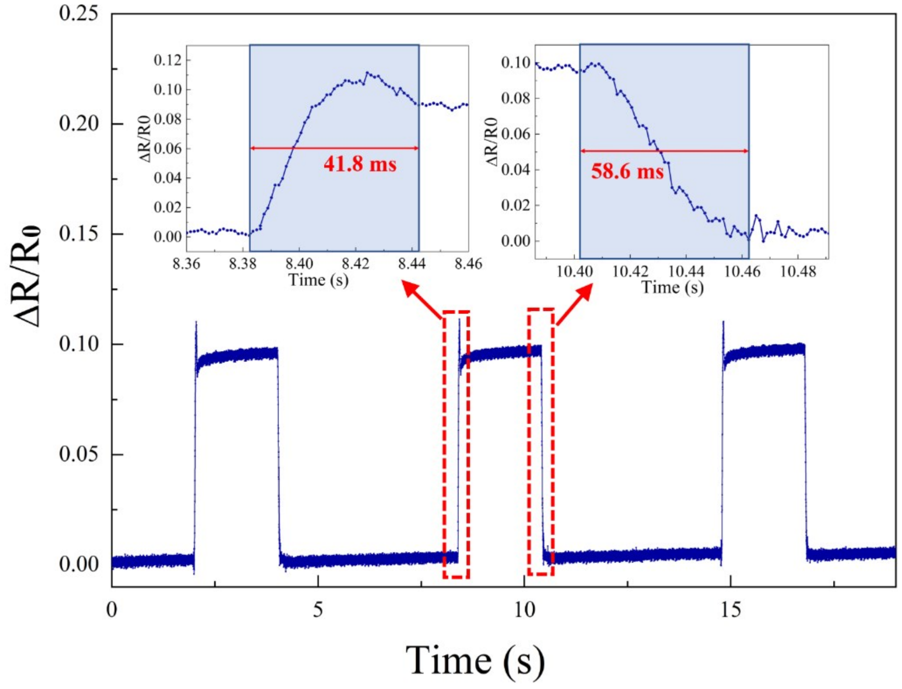

Figure S8. Response time of the GS-CNTS. The insets are the enlarged views during the loading and unloading stress stages.

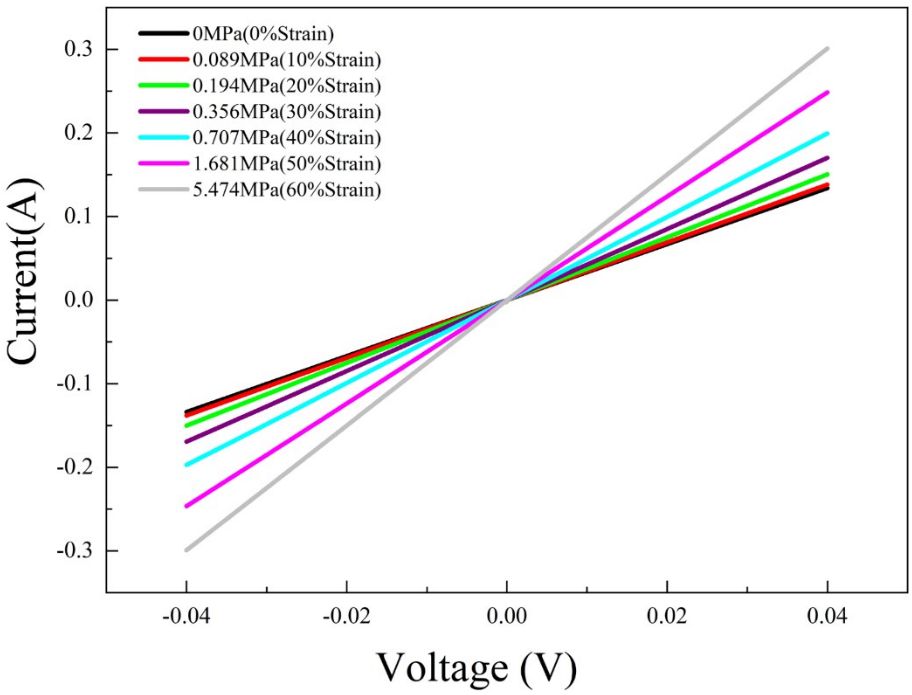

Figure S9. I-V curves of the GS-CNTS with various applied stress.

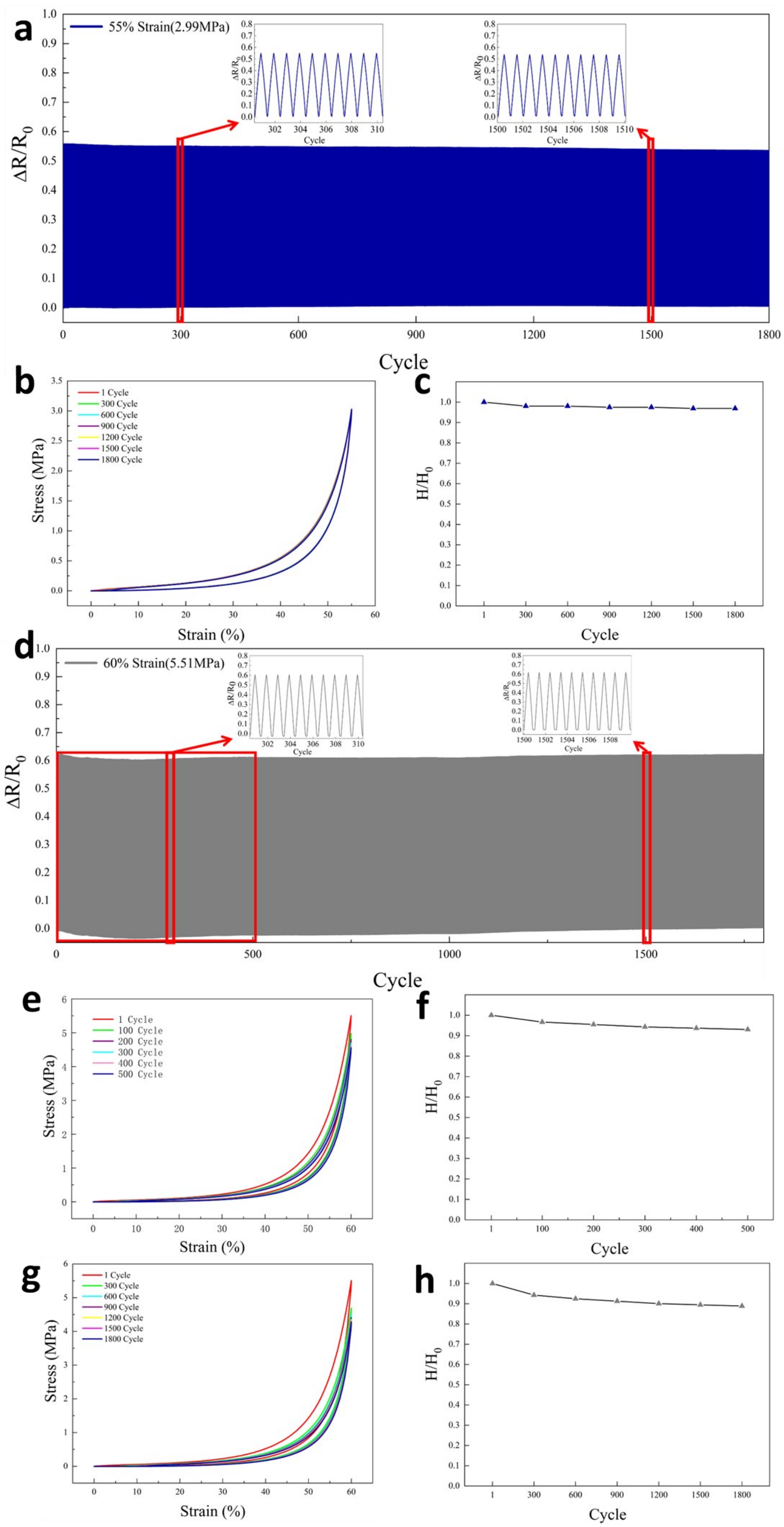
a
55% Strain(2.99MPa)
ΔR/R0
Cycle
b
Stress (MPa)
Strain (%)
1 Cycle
300 Cycle
600 Cycle
900 Cycle
1200 Cycle
1500 Cycle
1800 Cycle
c
H/H0
d
60% Strain(5.51MPa)
e
100 Cycle
200 Cycle
400 Cycle
500 Cycle
f
g
h

Figure S10. Working stability test of the GS-CNTS under high stress conditions. (**a**) $\Delta R/R_0$-cycle curve of the GS-CNTS with compression stress of 2.99 MPa (55% strain) for 1800 cycles. The insets are the enlarged views around 300th and 1500th cycles. (**b**) Stress-strain curves of the GS-CNTS with compression strain of 55% at the 1st, 300th, 600th, 900th, 1200th, 1500th, 1800th cycles. (**c**) Under 2.99MPa, the height change of the GS-CNTS after 1, 300, 600, 900, 1200, 1500, 1800 cycles of testing. H_0 is the initial height of the GS-CNTS, and H is the height of the GS-CNTS after test the compression-recover cycles. (**d**) $\Delta R/R_0$-cycle curve of the GS-CNTS with compression stress of 5.51 MPa (60% strain) for 1800 cycles. The insets are the enlarged views around 300th and 1500th cycles. (**e**) Stress-strain curves of the GS-CNTS with compression strain of 60% at the 1st, 100th, 200th, 300th, 400th, 500th cycles. (**f**) Under 5.51MPa, the height change of the GS-CNTS after 1, 100, 200, 300, 400, 500 cycles of testing. (**g**) Stress-strain curves of the GS-CNTS with compression strain of 60% at the 1st, 300th, 600th, 900th, 1200th, 1500th, 1800th cycles. (**h**) Under 5.51MPa, the height change of the GS-CNTS after 1, 300, 600, 900, 1200, 1500, 1800 cycles of testing.

Table S1. Comparison of the main parameters of the pressure sensor in this work and the previous work

Materials	Detection limit	Max stress	Sensitivity	Film or sponge	Type	Reference
MXene/tissue paper	10.2 Pa	30 kPa	0.55 kPa^{-1}(0.023-3.036 kPa),3.81 kPa^{-1} (3.036-10 kPa)	Film	Resistive	[1]
CNT/PI	10 Pa	61 kPa	11.28 kPa^{-1} (0-5 kPa),0.33 kPa^{-1} (15-60 kPa)	Sponge	Resistive	[2]
Carbonyl iron/ PDMS/AgNW	2 Pa	200 kPa	0.28 kPa^{-1} (0-10 kPa),0.02 kPa^{-1} (50-200 kPa)	Film	Capacitive	[3]
AgNP/PDMS	4.1 Pa	200 kPa	50mV kPa^{-1} (4.1Pa-8 kPa),1.8 mV kPa^{-1} (8 kPa-115 kPa),0.8 mV kPa^{-1} (115 kPa-200 kPa)	Sponge	Piezo-thermic	[4]
rGO/PVDF	1.3 Pa	353 kPa	47.7 kPa^{-1}	Film	Resistive	[5]
PVA/H_3PO_4	0.08Pa	360 kPa	3.3 Pa^{-1} (0-10 kPa),671.7 kPa^{-1} (10-100 kPa),229.9 kPa^{-1} (100-360 kPa)	Film	Capacitive	[6]
GO/rGO/PDMS	500 Pa	450 kPa	2×10^{-3} kPa^{-1} (0.5-10 kPa),3×10^{-5} kPa^{-1} (10-450 kPa)	Film	Capacitive	[7]
TPV/Ni/ PET/ITO	1 Pa	500 kPa	1×10^{6} kPa^{-1} (1Pa-20 kPa),3.1×10^{4} kPa^{-1} (20 kPa-500 kPa)	Film	Resistive	[8]
CNT/PDMS	10 Pa	1.2 MPa	0.01-0.02 kPa^{-1}	Sponge	Resistive	[9]
Graphene/ PDMS/AgNW	250 Pa	3 MPa	2.05×10^{-4} kPa^{-1} (0.25-500 kPa),9.43×10^{-6} kPa^{-1} (500-3000 kPa)	Film	Resistive	[10]
Gradient stiffness cabon nanotube sponge	2.2 kPa	5.47 MPa	0.765 MPa^{-1} (0.1-0.49 MPa),0.027 MPa^{-1} (1.97-5.47 MPa)	Sponge	Resistive	**This work**

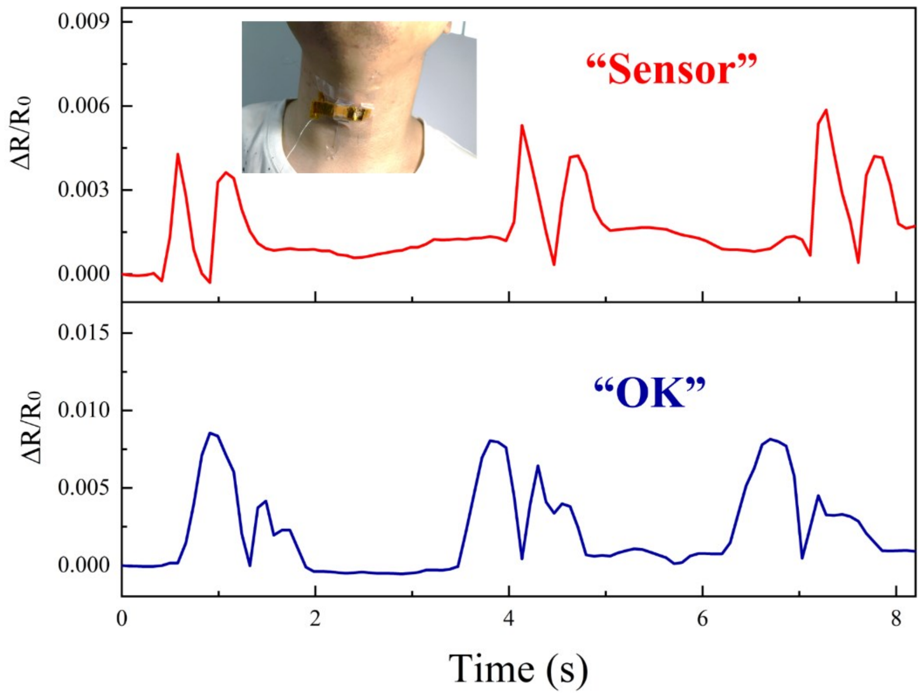

Figure S11. The $\Delta R/R_0$-time curve of the GS-CNTS when attached to the throat.

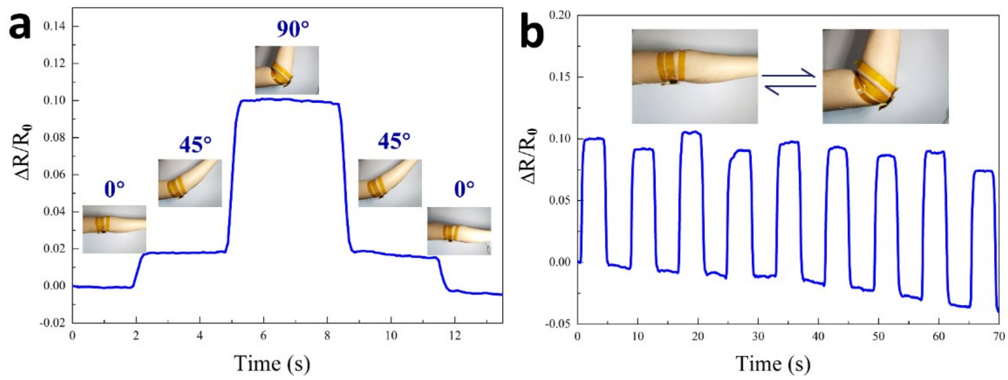

Figure S12. The $\Delta R/R_0$-time curve of the GS-CNTS when attached to the elbow.

Supplementary Movies

Movie S1. The process of falling the ball on the SS-CNTS.

Movie S2. The process of falling the ball on the GS-CNTS.

Movie S3. The mechanical fingers gently pick up the fragile hollow fries.

1 Y. Guo, M. Zhong, Z. Fang, P. Wan and G. Yu, *Nano letters* 2019, **19**, 1143.

2 X. Chen, H. Liu, Y. Zheng, Y. Zhai, X. Liu, C. Liu, L. Mi, Z. Guo and C. Shen, *ACS*

applied materials & interfaces 2019, **11**, 42594.

3 Q. Zhou, Bing Ji, Y. Wei, B. Hu, Y. Gao, Q. Xu, J. Zhou and B. Zhou, *Journal of materials chemistry A* 2019, **7**, 27334.

4 S. Zhao and R. Zhu, *Adv. Mater. Technol.* 2019, **4**, 1900414.

5 Y. Lee, J. Park, S. Cho, Y.-E. Shin, H. Lee, J. Kim, J. Myoung, S. Cho, S. Kang, C. Baig and H. Ko, *ACS nano* 2018, **12**, 4045.

6 N. Bai, L. Wang, Q. Wang, J. Deng, Y. Wang, P. Lu, J. Huang, G. Li, Y. Zhang, J. Yang, K. Xie, X. Zhao and C. F. Guo, *Nature communications* 2020, **11**, 209.

7 D. H. Ho, Q. Sun, S. Y. Kim, J. T. Han, D. H. Kim and J. H. Cho, *Adv. Mater.* 2016, **28**, 2601.

8 K. Tian, G. Sui, P. Yang, H. Deng and Q. Fu, *ACS applied materials & interfaces* 2020, **12**, 20998.

9 S. Kim, M. Amjadi, T.-I. Lee, Y. Jeong, D. Kwon, M. S. Kim, K. Kim, T.-S. Kim and Y. S. Oh, I. Park, *ACS applied materials & interfaces* 2019, **11**, 23639.

10 S.-H. Shin, S. Ji, S. Choi, K.-H. Pyo, B. Wan An, J. Park, J. Kim, J.-Y. Kim, K.-S. Lee, S.-Y. Kwon, J. Heo, B.-G. Park and J.-U. Park, *Nature communications* 2017, **8**, 14950.